IEEE Access
Multidisciplinary | Rapid Review | Open Access Journal

Received 26 August 2025, accepted 2 September 2025, date of publication 4 September 2025,
date of current version 10 September 2025.

Digital Object Identifier 10.1109/ACCESS.2025.3606368

RESEARCH ARTICLE

A Simplified Disturbance Detector Approach Based on Self-Adjusting Thresholds

SÓLON S. OTOMURA, MOISÉS J. B. B. DAVI, MATHEUS DO VAL OLIVEIRA, JOSÉ C. M. VIEIRA, (Member, IEEE), AND MÁRIO OLESKOVICZ, (Member, IEEE)
Department of Electrical and Computer Engineering, University of São Paulo, São Carlos 13566-590, Brazil

Corresponding author: Sólon S. Otomura (solon.otomura@usp.br)

This work was supported in part by Brazilian Federal Agency for Support and Evaluation of Graduate Education (CAPES); in part by Sao Paulo Research Foundation (FAPESP) under Grant 2024/17884-3; in part by the National Council for Scientific and Technological Development (CNPq); in part by the Research Center for Greenhouse Gas Innovation (RCGI) hosted by the University of São Paulo (USP) sponsored by FAPESP under Grant 2020/15230-5; and in part by TotalEnergies and the Strategic Importance of the support given by Brazil's National Oil, Natural Gas, and Biofuels Agency (ANP) through the Research, Development, and Innovation (R&DI) Levy Regulation.

ABSTRACT The increasing prevalence of Inverter-Based Resources (IBRs) in modern power systems introduces new challenges to conventional fixed-threshold fault detection methods, which often lack adaptability and robustness under varying system topologies, noise levels, and signal resolutions. In this context, this paper presents a novel disturbance detection methodology that combines the simplicity of a low-cost signal processing technique with an adaptive thresholding-based detection logic. The method relies on the modulus of incremental current and employs self-adjusting thresholds derived from Mathematical Morphology. Extensive validation is conducted through simulations on a detailed real-world wind farm model comprising 120 full-converter turbines and 27,900 distinct fault scenarios. The simulation set includes variations in fault type, resistance, and inception angle, as well as the operating power factor and generation level of the wind farm. The proposed approach consistently achieves high accuracy, above 99%, across all scenarios, maintaining resilience under challenging signal-to-noise ratios as low as 40 dB and reduced sampling rates down to 16 points per cycle, without requiring system- or scenario-specific threshold tuning. Comparative analyses with conventional fixed-threshold techniques, including Sample-by-Sample, Cumulative Sum, and Current-Slope Based methods, highlight the superior robustness, accuracy, security, and deployment potential of the proposed method. Furthermore, processing benchmarks demonstrate a computational time reduction of approximately 99% compared to more complex techniques such as Wavelet Transform and entropy-based analysis, reinforcing its suitability for embedded and real-time protection systems.

INDEX TERMS Adaptive threshold, fault detection, inverter-based resources, mathematical morphology, wind farm.

I. INTRODUCTION

The increasing penetration of renewable energy sources, driven by global sustainability goals, has led to a growing presence of Inverter-Based Resources (IBRs) in electrical power systems. Among these, Doubly Fed Induction Generators and Full Converter Generators stand out in wind power generation. These IBRs exhibit distinct transient behavior due to their inherent power-electronic control systems, with differ significantly from those of conventional synchronous generators [1], [2]. Consequently, this difference affects conventional protection schemes [3], [4], which require more sophisticated methods to ensure system reliability and security. Beyond impacts on protection schemes, fault diagnosis methods that encompass fault detection [5], classification [6], and location [7] have also been the focus of studies related to the impact of IBRs on the power system.

The associate editor coordinating the review of this manuscript and approving it for publication was Diego Bellan.

In general, fault detection methods are typically based on extracting features from current variations and comparing them with fixed detection thresholds previously set by the protection engineer [8], [9], [10]. While such techniques are well established, their reliance on fixed thresholds represents a limitation, especially in systems with IBRs. In these scenarios, the variability of operating conditions and the noise introduced by power-electronic interfaces can compromise detection consistency.

In response to the limitations of traditional fixed-threshold techniques, more sophisticated signal processing strategies have emerged, such as the Stockwell Transform combined with Decision Trees [11] and the Wavelet Transform [12]. Despite their technical merits, these methods typically still rely on fixed detection thresholds, which may limit their adaptability to varying operating conditions.

This limitation becomes relevant in systems predominantly composed of IBRs, where signal variability and noise introduced by power-electronic interfaces create additional detection challenges. To address these issues, recent studies have proposed detection methodologies designed explicitly for IBR-based systems. Among them, [13] and [14] present solutions based on the Discrete Wavelet Transform (DWT) that also depend on fixed thresholds. However, they do not evaluate a broad set of fault scenarios such as varying fault resistance, inception angle, and location, and omit analysis of detection sensitivity under noisy conditions. As a result, the generalizability and reliability of these thresholds remain uncertain.

As an alternative, adaptive thresholding techniques have been proposed to partially overcome the shortcomings of fixed-threshold methods, as demonstrated by [15]. However, these approaches often still incorporate fixed safety margins, limiting their capacity to fully adapt to changing system behavior.

To address these limitations, this paper proposes a novel methodology for fault detection in systems with IBRs, based on the modulus of incremental currents and adaptive thresholds defined using Mathematical Morphology. This work targets internal faults within wind farm collector systems explicitly, a scenario that poses challenges due to the distributed nature of generation and to the variability of system operating conditions, which remains underexplored in the literature. The proposed approach features a simplified signal processing structure that ensures high detection performance while maintaining low computational complexity, making it suitable for practical applications without the need for manual parameter tuning.

The main contributions of this paper can be summarized as follows:

- Novel, computationally efficient self-adjusting disturbance detector for systems with IBRs: This paper proposes a new disturbance detection methodology featuring a robust and simplified low-complexity signal processing structure suitable for practical deployment. The method relies on incremental current modulus calculations and Mathematical Morphology techniques to define adaptive detection thresholds, maintaining high sensitivity and accuracy without requiring scenario-specific parameter tuning. The adaptive thresholding strategy adopts the concept of a previously validated approach [5]. Still, the signal processing technique has been redesigned to improve efficiency and applicability.
- Comprehensive and realistic benchmarking of fault detection algorithms applied in wind farm collector systems: Although most recent studies focus solely on faults occurring on IBR interconnection transmission lines, this work pioneers a large-scale evaluation of disturbance detection methods specifically for internal wind farm collector systems. This context remains insufficiently explored in the literature. In this research, the assessment considers a wide range of fault scenarios, including variations in fault type, resistance, inception angle, location, and operating conditions.

TABLE 1. Parameters considered in the evaluation to reflect diverse operating conditions and fault scenarios.

Fault Parameter	
Fault type	AG, BG, CG, AB, BC, CA, ABG, BCG, CAG, ABC
Fault resistance	0, 10, 25, 40, 50 Ω
Inception angle	0, 45, 90°
Fault location	$F1$ to $F31$ (Fig. 1)
Operation Parameter	
Generation level	0.1, 0.75 p.u.
Power factor	1.0, 0.95 capacitive, 0.95 inductive
Measurement points	P_{C1}, P_{C2}, P_{C3}, P_{C4} (Fig. 1)

This paper presents a structured investigation into the development and validation of the proposed disturbance detector approach. The following sections are organized to progressively support this objective. Section II introduces the real-world test system and simulation set-up used throughout the study. Section III evaluates the performance of conventional detection methods, establishing a comparative baseline. Section IV details the proposed methodology, including its formulation and processing stages. Section V presents a comprehensive performance assessment, highlighting improvements over existing techniques. Finally, Section VI provides concluding remarks.

II. TEST SYSTEM

For this analysis, a wind farm based on IBRs was modeled in the PSCAD simulation environment. Fig. 1 presents the single-line diagram along with the parameters of the test system, which corresponds to a real-world wind power plant.

The system consists of four primary collector busbars (C1, C2, C3 and C4), integrating a total of 120 full-converter wind turbines. To minimize computational burden in simulations, one circuit per collector bus was modeled in detail, while

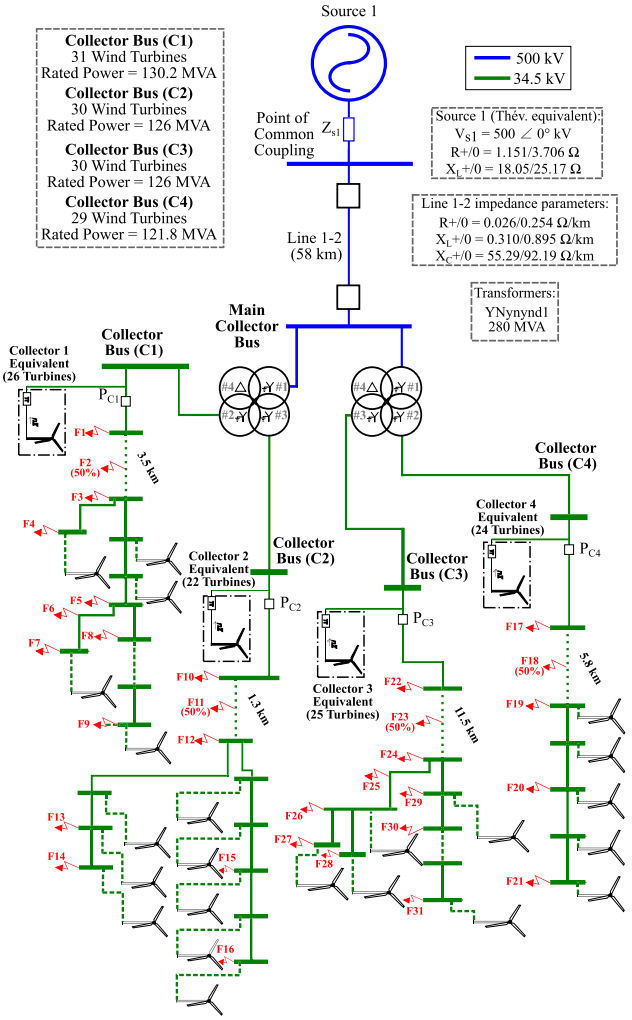

FIGURE 1. Single-line diagram of the test system, including measurement points (P_{C1}, P_{C2}, P_{C3}, and P_{C4}), fault application locations ($F1$ to $F31$), and main parameters.

the remaining circuits were represented using an equivalent model, following the methodology described in [16].

A comprehensive set of fault scenarios, with the corresponding fault and operating parameters summarized in Table 1, was simulated within the collector system to evaluate the performance of disturbance detection methods.

The fault locations were assigned at 0%, 50%, and 100% of the collector lines in the detailed circuits and additional fault positions were distributed among other buses within each collector circuit, covering conductor sections ranging from 50 to 300 m, which are also shown in Fig. 1. Fault simulations were performed at predefined locations, incorporating variations in fault types, fault resistance, and fault inception angle. Furthermore, different levels of wind power plant generation were considered, and the simulations assumed full converter generators operating at three different power factor. Given the variations in the characteristics of the fault and the generation levels, a total of 27,900 scenarios were analyzed. Measurements were taken at the entrance of the detailed circuits, with an initial sampling rate of 256 points per cycle (ppc) and a system frequency of 60 Hz.

III. PERFORMANCE LIMITATIONS OF EXISTING METHODS

To highlight the limitations of conventional disturbance detection techniques in IBR-based systems, three widely cited techniques are evaluated: Sample-by-Sample (SBS) [10], Cumulative Sum (CUSUM) [8], and Current-Slope Based (CSB) [9]. These methods, commonly used in systems without IBRs, are applied to a large set of fault scenarios in the tested wind farm collector system.

A brief description of each method is presented below, followed by a performance comparison under different Signal-to-Noise Ratio (SNR) and sampling frequencies.

A. EVALUATED METHODS

1) SBS

Identifies abrupt variations in current magnitude by computing the absolute difference between consecutive samples. A disturbance is detected when this difference exceeds a predefined threshold for more than three consecutive samples [10].

2) CUSUM

Applies a two-sided cumulative approach to detect abrupt changes in the current signal $s(k)$ [8]. Two auxiliary sequences are defined: $s_1(k)$ and $s_2(k)$, representing the direct and inverted forms of the original signal, respectively:

$$s_1(k) = s(k), \quad s_2(k) = -s(k) \tag{1}$$

Based on these sequences, two cumulative indices $g_1(k)$ and $g_2(k)$ are computed recursively. The parameter v is a drift term, typically set to the maximum (peak) value of the current under nominal conditions [8]. The equations are given by:

$$g_1(k) = \max\left(g_1(k-1) + s_1(k) - v,\ 0\right) \tag{2}$$

$$g_2(k) = \max\left(g_2(k-1) + s_2(k) - v,\ 0\right) \tag{3}$$

A disturbance is detected when $g_1(k)$ or $g_2(k)$ exceeds a fixed threshold for more than three consecutive samples [8].

3) CSB

Detects faults by monitoring the cumulative rate of change of the current signal over a one-cycle window. The slope between consecutive samples is first computed as:

$$d(k) = \frac{i(k) - i(k-1)}{\Delta t} \tag{4}$$

where $i(k)$ is the current sample at time k, and Δt is the sampling interval. The fault index $S(k)$ is then calculated as the sum of the slopes over one cycle:

$$S(k) = \sum_{l=k-N+1}^{k} d(l) \tag{5}$$

Alternatively, this index can be expressed recursively as:

$$S(k) = S(k-1) + \frac{i(k) - i(k-1)}{\Delta t} \tag{6}$$

TABLE 2. Threshold values for each method under sensitivity, balanced, and security configurations.

Threshold Sensitivity Level	SBS	CUSUM	CSB
High Sensitivity Treshold	0.03 p.u.	0.001 p.u.	100
Balanced Threshold	0.1 p.u	0.01 p.u.	1000
High Security Threshold	0.6 p.u.	0.5 p.u.	10000

A fault is detected when the absolute value of $S(k)$ exceeds a predefined threshold for more than three consecutive samples [9].

4) EVALUATION CRITERIA

In the following sections, each method was evaluated using three threshold (TH) configurations: a lower value focused on sensitivity, an intermediate value representing a balanced operating point between sensitivity and security, and a higher value aimed at enhancing security and avoiding false detections during the pre-fault periods.

The intermediate values were determined after preliminary tests with the simulated waveforms to favor the performance of traditional methods. The other values were increments or decrements of the intermediate value, designed to emphasize the sensitivity and security characteristics of traditional methods.

Table 2 summarizes the threshold values adopted for each method in the sensitivity, balanced, and security configurations.

Detection accuracy is defined as the ratio of correctly identified faults to the total number of evaluated cases. A detection is considered successful if it occurs within 100 ms after fault inception and if it is triggered by the protection device located at the faulted circuit. Early detections or those not triggered within this window are classified as failures.

B. PERFORMANCE EVALUATION UNDER DIFFERENT SIGNAL-TO-NOISE RATIO CONDITIONS

The performance of the methods was analyzed under two SNR conditions: 60 dB, representing a near-ideal measurement environment, and 40 dB, simulating a scenario with more significant but realistic noise interference [17], [18]. To simulate these disturbances, additive white Gaussian noise was applied to the three-phase current signals, enabling a controlled analysis of the method's behavior under varying levels of measurement noise. A summary of the detection performance in these scenarios is presented in Fig. 2.

Although CSB maintained perfect accuracy under low noise conditions, its performance proved highly sensitive to the chosen threshold when exposed to increased noise. While it remained highly reliable with *Balanced* and *High Security* TH, its detection capability collapsed under *High Sensitivity* TH, triggering false positives for all cases. SBS and CUSUM, on the other hand, showed a gradual decline in performance. SBS demonstrated consistent but modest accuracy degradation, revealing a strong dependency on the chosen TH across both noise levels. CUSUM exhibited a more pronounced loss of accuracy under noisy situations. Although it initially performed well with all three TH levels, its accuracy dropped significantly as *High Sensitivity TH* was applied under noisier conditions. These observations highlight the fragility of fixed-threshold methods when subjected to realistic variations in signal quality and the critical role of adaptive strategies in maintaining robust detection.

These results highlight the lack of robustness under of fixed-threshold approaches, whose performance is highly dependent on the appropriate tuning of thresholds and degrades under adverse conditions. Even under near-ideal environments, inadequate TH selection can lead to significant accuracy loss. In noisy situations, particularly with the *High Sensitivity* TH configuration, detection reliability is further compromised.

C. PERFORMANCE EVALUATION UNDER DIFFERENT SAMPLING FREQUENCY

The detection performance of conventional methods under varying sampling frequencies is presented in Fig.3. Sampling frequency is a critical parameter in digital protection systems, affecting signal resolution and, consequently, the accuracy and responsiveness of detection algorithms. This analysis evaluates how fixed-threshold methods respond to changes in signal resolution. Simulations were performed with additive white Gaussian noise (40dB SNR), and sampling rates of 256, 128, 64, 32, and 16 ppc covering a wide range of resolutions commonly found in protection and monitoring systems.

The SBS method showed strong dependence on sampling resolution and threshold selection. At the *High Sensitivity* TH (0.03p.u.), performance dropped from 90.61% at 256 ppc to 0% at lower rates. With the *Balanced* TH (0.1p.u.), accuracy remained high down to 64 ppc but dropped to 0% at 32 and 16 ppc. At the *High Security* TH (0.5p.u.), results were irregular, with accuracy recovering to 70.58% at 16 ppc. These results indicate that SBS is highly reliant on precise parameterization, which may limit its applicability.

CUSUM performed more consistently than SBS, especially with the *Balanced* TH (0.01 p.u.), maintaining over 84% accuracy down to 16 ppc. However, with the *High Sensitivity* TH (0.001 p.u.), accuracy dropped progressively, from 67.49% at 256 ppc to 32.25% at 16 ppc. This degradation reflects increased vulnerability to noise in low-resolution signals. The *High Security* TH (0.5 p.u.) showed inconsistent results, confirming CUSUM's dependence on appropriate threshold and resolution settings.

The CSB method achieved near-perfect performance for the *High Sensitivity* and *Balanced* THs (100 and 1000), even at 16 ppc. However, under the *High Security* TH (10,000), accuracy fell sharply with reduced sampling, reaching only 20.81% at 16 ppc. An anomalous result occurred for the *High Sensitivity* TH, where the method failed at 256 ppc but succeeded at lower resolutions. This behavior occurred

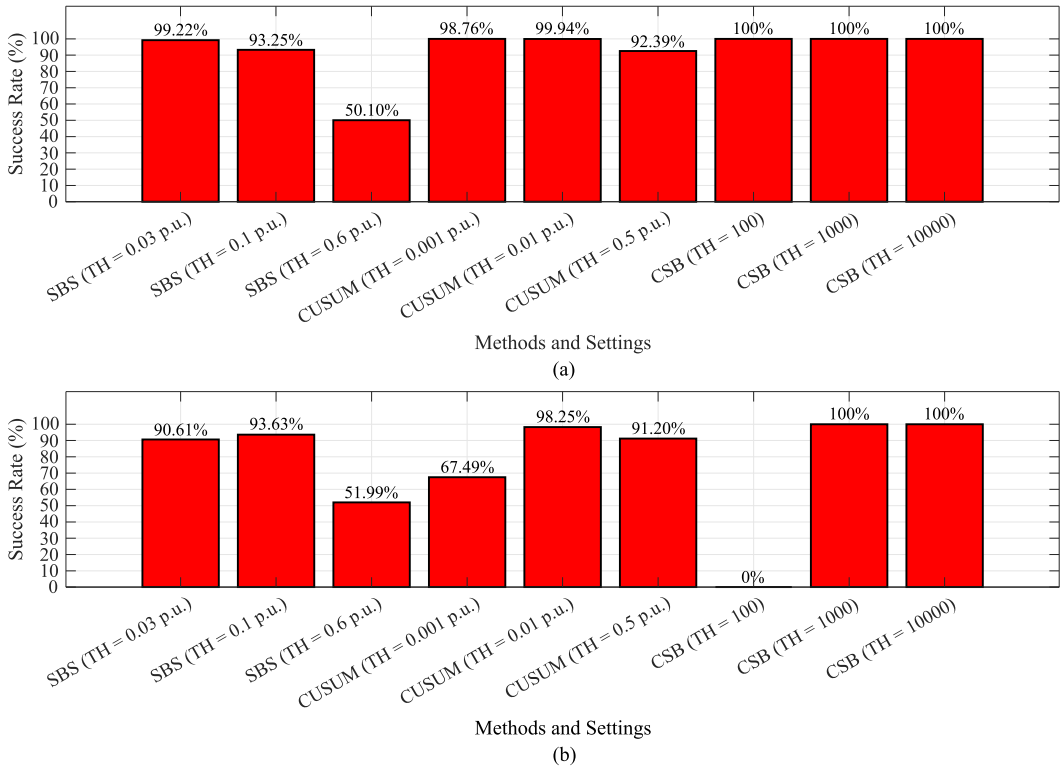

FIGURE 2. Detection performance of the SBS, CUSUM, and CSB methods for input signals with SNR of (a) 60 dB and (b) 40 dB.

due to the amplification of discrete slope values at lower sampling rates. These irregularities suggest that the CSB requires empirical tuning, which undermines its reliability under varying conditions.

D. GENERAL LIMITATIONS AND DEPLOYMENT CHALLENGES

All evaluated methods demonstrated a strong dependency on the threshold configuration, with detection performance deteriorating notably in the presence of noise and at lower sampling rates. Except for specific cases such as the CSB method under balanced threshold settings, most configurations failed to deliver consistently high accuracy, highlighting the challenge of maintaining reliable detection across scenarios. These limitations are particularly relevant in practical applications, such as the modeled wind farm collector system, where signal noise is expected due to the high-frequency switching of full converter. Signal resolution is constrained by the sampling rates typically supported by field-deployed relays. As a result, there is no generalizable threshold configuration that ensures robust performance across operating conditions, making fixed-threshold methods less suitable for systems subject to such variability.

IV. PROPOSED FAULT DETECTOR

This section introduces a novel fault detection methodology based on self-adjusting thresholds, designed to address the limitations of conventional fixed-threshold techniques. The method combines an adaptive thresholding strategy with a simplified signal processing technique to ensure high detection reliability while maintaining low computational complexity. Although it follows the concept of the adaptive thresholding principle presented in [5], the proposed approach was developed with a distinct design that maintains generalization capability and enhances practical applicability to different systems.

The methodology integrates two signal processing techniques: incremental current modulus calculation and mathematical morphology and these techniques are embedded in a six-stages decision-making process. The following subsections provide further details and references on the processing techniques, as well as a step-by-step description of the decision-making process.

A. INCREMENTAL CURRENT MODULUS CALCULATION

The proposed method employs the incremental current modulus as a computationally efficient signal processing technique, used to emphasize signal variations that are typically associated with fault events. The method relies solely on three-phase current measurements and calculates the difference between the present sample and the corresponding sample from the previous cycle [19]. To eliminate polarity dependence and ensure consistent detection across both positive and negative half-cycles, the modulus is applied to the resulting incremental current, as defined in (7).

$$\Delta i(t) = |i(t) - i(t - T)| \tag{7}$$

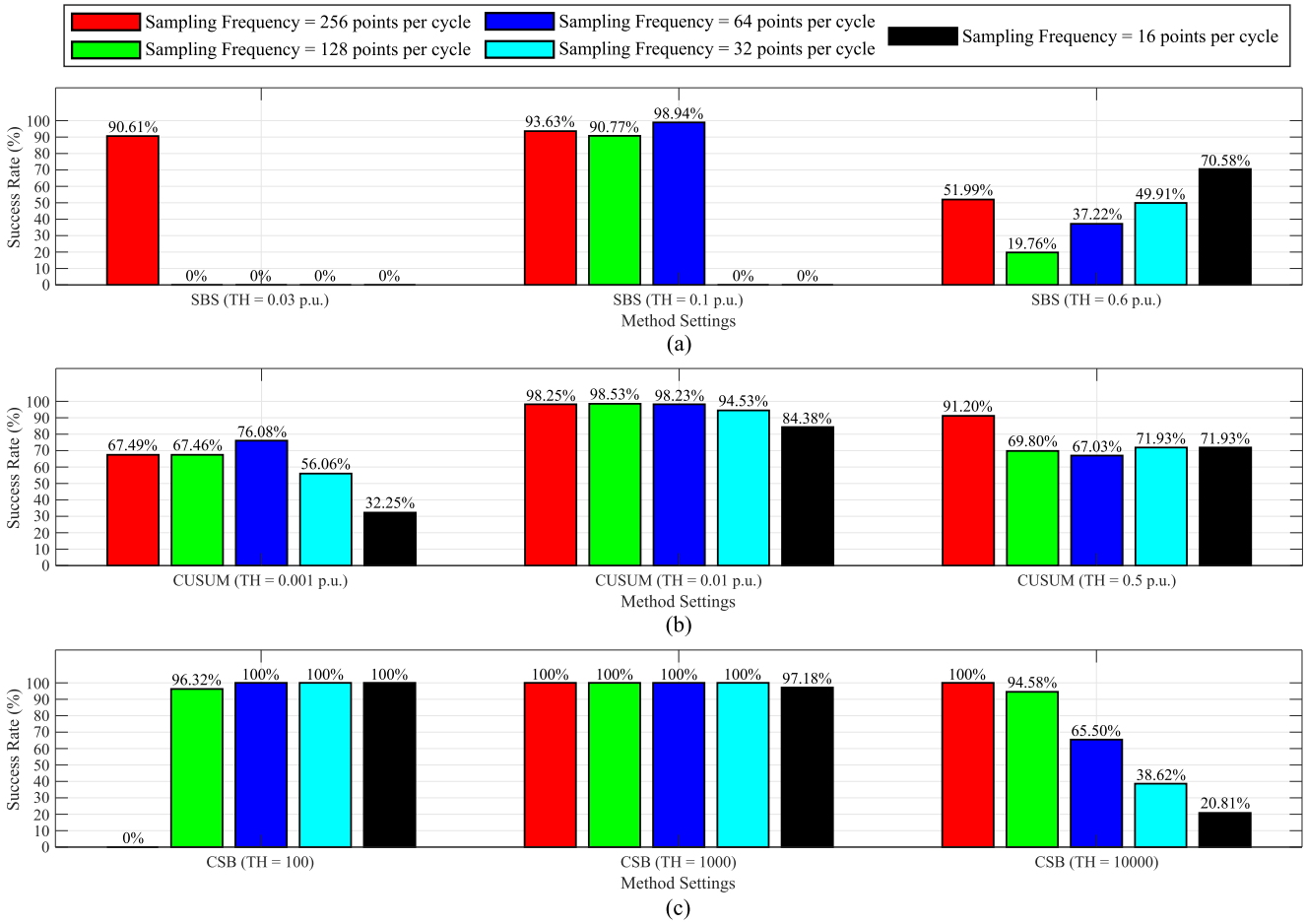

FIGURE 3. Detection performance under SNR of 40 dB and different sampling rates and threshold settings for (a) SBS, (b) CUSUM, and (c) CSB.

where, $\Delta i(t)$ is the instantaneous incremental current modulus at time t, T is the period of the fundamental cycle, $i(t)$ is the instantaneous current, and $i(t-T)$ is the corresponding instantaneous current from the previous cycle.

The incremental current modulus serves as the primary input to the detection logic, as shown in Fig. 4(b), where it is continuously evaluated against an adaptive threshold defined using Mathematical Morphology. This comparison forms the basis of the disturbance identification process, enabling the method to respond dynamically to variations in system conditions. The formulation and operation of the adaptive threshold are detailed in the following subsection.

B. ADAPTIVE THRESHOLDING USING MATHEMATICAL MORPHOLOGY (MM)

To define the adaptive threshold used in the detection process, the proposed method employs MM. This nonlinear framework can extract structural features from signals using morphological operators [20]. Among the available morphological operations, dilation is suitable for generating upper envelopes that track the signal's shape while consistently remaining above it [5], making it ideal for defining a dynamic, parameter-free threshold.

In MM, a *Structuring Element* slides across the signal, modifying its values based on the local neighborhood defined by the *element*'s shape and size. The dilation operator, as formulated in [20], represents the result of applying a Structuring Element $g(m)$ to a discrete signal $f(n)$ as shown in (8).

$$y(n) = (f \oplus g)(n) = \max \left\{ \begin{matrix} f(n-m) + g(m), \\ 0 \le (n-m) \le n, \\ m \ge 0 \end{matrix} \right\} \quad (8)$$

A flat, linear *Structuring Element* is adopted to ensure that the resulting envelope is both smooth and stable [5]. This envelope, obtained by applying the dilation operation to the incremental current modulus, serves as the adaptive threshold used in the detection logic. To prevent false positive detection under noisy conditions, an adaptive safety margin (SM) [5], defined in (9), is multiplied by the envelope.

$$SM = 1 + \left(\frac{V_{max} - V_{min}}{V_{mean}} \right) \quad (9)$$

In this expression, V_{max}, V_{min}, and V_{mean} correspond to the maximum, minimum, and mean values, respectively, obtained from the pre-fault samples of the incremental

current modulus. An illustration of the resulting adaptive threshold, including the applied safety margin, is presented in Fig. 4(c).

C. DECISION-MAKING LOGIC FOR FAULT DETECTION

The fault detection logic is structured into six main stages, combining the signal processing techniques previously introduced with a sequential evaluation strategy designed to balance sensitivity, robustness, and detection security. While the incremental current modulus emphasizes fault-related signal variations and the adaptive thresholding logic based on MM enhances noise resilience and adapts to varying operating conditions, security against false positive detection is ensured by the multi-stage decision-making process that validates the signal behavior before triggering a detection. The stages are as follows:

1) **Signal Acquisition:** The three-phase system currents are continuously measured to provide the raw input for the detection logic, as illustrated in Fig. 4(a).
2) **Incremental Current Modulus Calculation:** [19] The modulus of the difference between current samples and the corresponding sample from one cycle earlier is calculated to highlight signal variations associated with faults, as shown in Fig. 4(b).
3) **Threshold Definition via Dilation:** [20] The modulus signal is processed using the dilation operation of the MM to generate an upper envelope that dynamically adapts to the signal shape.
4) **Application of Adaptive Safety Margin:** The threshold is scaled by a *SM*, defined by (9), derived from the pre-fault signal profile, increasing robustness against noise, as depicted in Fig. 4(c).
5) **Threshold Delay:** [5] The resulting threshold is delayed by one fundamental cycle to ensure it reflects the system's previous steady-state conditions. This prevents the threshold from adapting to the disturbance itself and preserves the contrast needed for effective detection, as illustrated in Fig. 4(d).
6) **Decision Logic:** A fault is detected when the incremental modulus exceeds the delayed adaptive threshold for six consecutive samples.

The waveforms shown in Fig. 4 illustrate the main stages of the proposed detection method, using a representative fault current signal. The diagram highlights how the incremental current modulus is used as the primary feature to track signal variations. At the same time, the adaptive threshold, defined through the dilation operation of MM, ensures responsiveness to the signal's shape without requiring manually tuned parameters. The threshold is further scaled by an adaptive safety margin to suppress noise-induced fluctuations and then delayed by one cycle to maintain alignment with the system's past operating condition. This combination enables the detection logic to operate with high sensitivity to disturbances while maintaining robustness against noises and security against false positives.

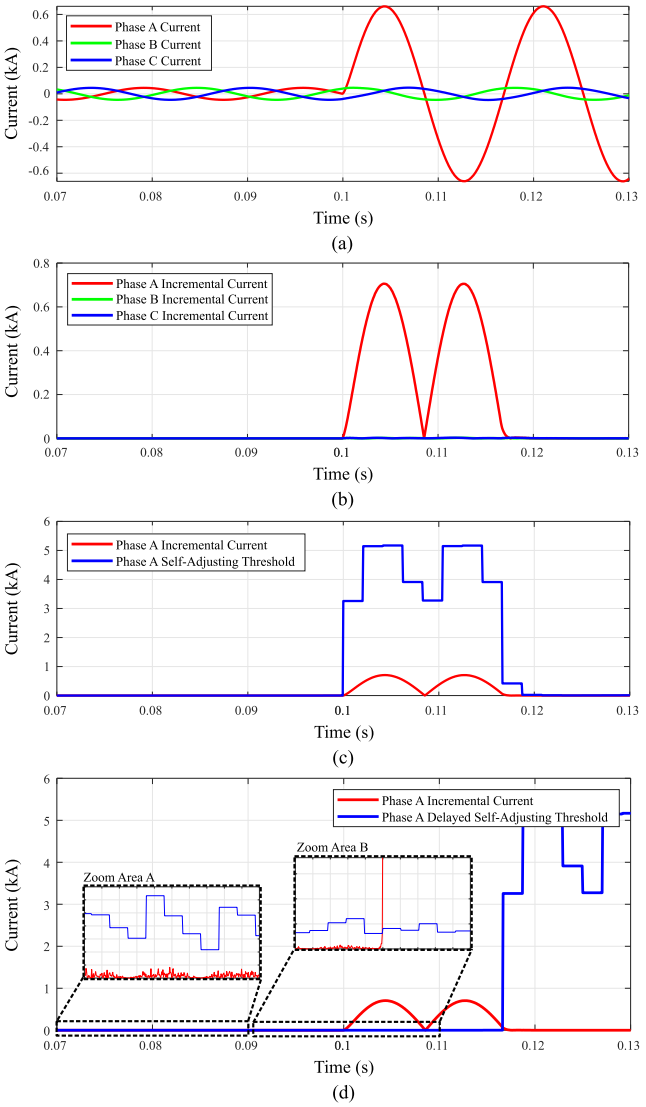

FIGURE 4. Example of the waveforms obtained in the different processing stages of the proposed method for a AG fault: (a) phase currents, (b) modulus of the incremental phase currents, (c) self-adjusting threshold along with the incremental current for the faulted phase, (d) delayed self-adjusting threshold along with the incremental current for the faulted phase (used for the method's decision-making).

V. PROPOSED FAULT DETECTOR PERFORMANCE ASSESSMENT

The performance of the proposed fault detection method was evaluated using the same comprehensive simulation dataset applied to conventional methods. This ensures a consistent and fair comparison across all approaches. All 27,900 test cases were considered, encompassing variations in fault type, resistance, inception angle, location, as well as system operating conditions.

As with the evaluation of conventional fixed-threshold methods, two main assessments were carried out for the proposed approach, focusing on conditions that are particularly critical in IBR-based systems: noise resilience and signal resolution.

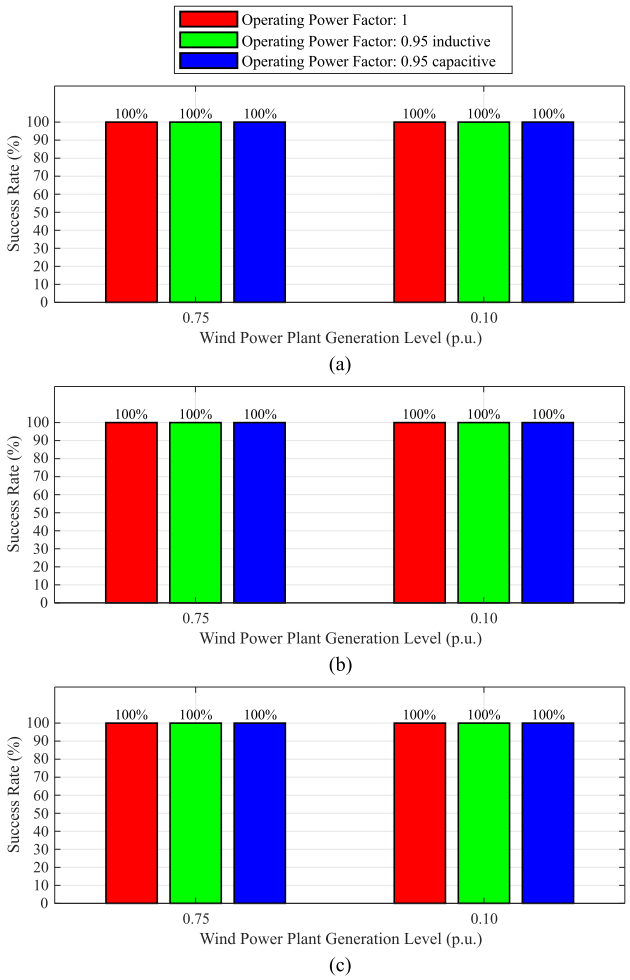

FIGURE 5. Performance evaluation of the proposed method under SNR conditions of (a) 60 dB, (b) 50 dB, and (c) 40 dB.

A. PERFORMANCE EVALUATION UNDER DIFFERENT SNR CONDITIONS

The first assessment investigates robustness under SNR of 60, 50, and 40 dB, with the intermediate level (50 dB) included to provide a more detailed characterization of noise effects. To highlight the adaptive threshold method's performance under different wind farm operating conditions, including variations in power factor and generation penetration, the results are detailed per operating configuration. Unlike the evaluation of conventional methods, where results were presented as overall values across all conditions, this breakdown provides clearer insight into the proposed method's consistency across scenarios. The detailed detection performance is shown in Fig. 5.

The method achieved 100% detection accuracy across all test scenarios, regardless of the SNR level, the operating power factor, or the power generation level. Even under the most adverse condition of 40 dB SNR, no false detections or missed events were observed. This robustness stands in contrast to conventional fixed-threshold methods, which exhibited notable performance degradation under similar conditions, particularly when configured with high-sensitivity thresholds.

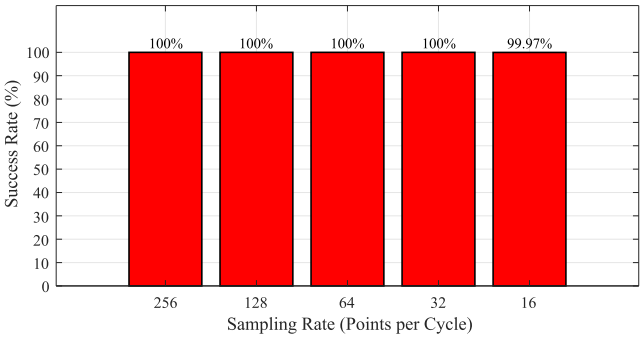

FIGURE 6. Detection performance of the proposed method for different sampling rates (points per cycle).

The superior performance stems from the method's adaptive thresholding mechanism, which adjusts to the system's operating state, along with the use of a dynamic safety margin and a requirement for six consecutive samples to confirm detection. These features ensure both responsiveness and reliability, preventing spurious triggers and guaranteeing detection even in challenging environments. The consistent results across all evaluated operating configurations reinforce the method's applicability to IBR-based systems, where noise and limited signal resolution are common constraints.

B. PERFORMANCE EVALUATION UNDER DIFFERENT SAMPLING FREQUENCY

The second assessment evaluates the adaptability of the proposed method under different sampling conditions, simulations were carried out using five sampling rates: 256, 128, 64, 32, and 16 ppc. Although higher rates provide more detail of the signal, the lower values, particularly 64, 32 and 16 ppc, were selected to emulate the typical sampling rates found in practical relay-based protection systems.

The impact of the sampling rate on the performance of the proposed method is illustrated in Fig. 6, offering insight into its stability even under low resolution acquisition conditions.

The results presented in Fig. 6 consider only the unity power factor and the maximum penetration scenario. This choice is supported by the absence of significant performance variations across different operating conditions, as observed in previous Subsection V-A. Among all the cases evaluated, a single false detection occurred at a sampling rate of 16 ppc. This event involved a CAG-type fault, where detection was triggered during the pre-fault period.

This isolated case may be attributed to the combined influence of Gaussian noise randomness, low sampling frequency, and the use of only two pre-fault cycles to compute the adaptive safety margin in (9). In practical applications, extending the pre-fault window can improve the statistical representation of noise, increasing the robustness of the self-adjusting threshold.

TABLE 3. Performance comparison between proposed method and state-of-the-art techniques.

Performance Benchmark: Proposed vs. Existing Methods		
Method analysed	Accuracy	
	Best Scenario	Worst Scenario
SBS (TH = 0.1 p.u)	99.22%	0%
CUSUM (TH = 0.01 p.u)	99.94%	84.38%
CSB (TH = 1000)	100%	97.18%
Proposed Method (Adaptive TH)	100%	99.97%

C. PERFORMANCE HIGHLIGHTS

The proposed fault detection method consistently demonstrated high performance in all the scenarios evaluated. It achieved 100% detection accuracy under all tested SNR levels (60, 50, and 40 dB). The method also maintained robust performance at varying sampling frequencies, with a minimum success rate of 99.97% at the lowest resolution of 16 ppc.

Unlike conventional fixed-threshold methods, which showed significant sensitivity to threshold tuning, noise levels, and signal resolution, the proposed approach exhibited stable behavior without relying on empirical parameterization.

Table 3 presents the performance comparison between the proposed and existing methods. ''Best Scenario'' corresponds to tests conducted with 256 ppc and 60 dB SNR, while ''Worst Scenario'' refers to 16 ppc and 40 dB SNR. For the existing methods, the results shown correspond to the balanced threshold configuration, which yielded the best overall performance during testing.

These results reinforce the effectiveness of the simplified fault detection method and support its practical applicability, particularly in real-world systems characterized by limited signal resolution or elevated noise levels.

D. PROCESSING TIME COMPARISON

In order to demonstrate the practical feasibility of the proposed simplified disturbance detector, a processing time evaluation was carried out, comparing the performance of DWT/Entropy method [5] with the newly developed simplified method proposed in this paper. All tests were carried out using MATLAB software with the built-in `tic...toc` function to ensure precise measurement of computation times.

For both methods, the detection algorithm was executed 1000 times over the same set of three-phase signals, each with a duration of 400 ms. The timing encompassed all stages of both algorithms, including signal buffer initialization, signal processing stages, the construction of self-adjusting thresholds, and the comparison of these thresholds with the analyzed signals for disturbance detection. All experiments were performed on a workstation equipped with an AMD Ryzen 7 2700 CPU (3.20 GHz).

TABLE 4. Processing time using the DWT/Entropy and proposed methods.

Test	DWT/Entropy Method (ms)	Proposed Method (ms)
1	244.0489	3.4220
2	244.5549	3.5589
3	246.8935	3.3735
4	242.1069	3.3364
5	244.3525	3.5795

Five independent runs were performed for each approach (simplified and DWT/Entropy [5]). The processing time per execution, obtained for each run and for both methods, is summarized in Table 4.

The resulting average processing times for each method are 3.4541 ms for the proposed simplified version and 244.3913 ms for the base version.

As demonstrated in [5], the DWT/Entropy methodology has already been shown to be viable for practical implementation. However, the results obtained in this work highlight that the proposed simplified method yields a very significant reduction in processing time, achieving an improvement of approximately 98.6% over the base method. These findings reinforce the methodological choices made and expand the prospects for real-time or embedded applications where computational efficiency is critical.

VI. CONCLUSION

This work has presented a novel fault detection methodology designed for wind farm collector systems, combining computational efficiency with high detection performance. The proposed approach eliminates the need for complex signal processing techniques, such as wavelet decomposition and entropy analysis, by relying instead on the incremental current modulus. This simplified structure significantly reduces computational cost while maintaining high sensitivity and robustness under diverse fault conditions, noise environments, and sampling rates.

The methodology was validated through extensive simulations using a real wind farm model and compared against conventional fixed-threshold techniques, including SBS, CUSUM, and CSB. The results highlight the limitations of these traditional methods, which heavily depend on parameter tuning and exhibit instability under higher noise levels, and lower signal resolutions. In contrast, the proposed method achieves consistently high accuracy without requiring case-specific adjustments, demonstrating superior adaptability, reliability, and ease of implementation.

Moreover, the proposed solution achieves a processing time reduction of approximately 99% compared to prior adaptive methods, reinforcing its suitability for real-time and embedded protection systems. Overall, this work contributes a practical and generalizable strategy for disturbance detection, offering a favorable balance between sensitivity, robustness, security, and low computational demand.

REFERENCES

[1] M. J. B. B. Davi, D. C. Jorge, and F. V. Lopes, "Fault current and fault voltage analysis of power transmission systems with high penetration of inverter-based wind generators," *Acta Scientiarum. Technol.*, vol. 44, May 2022, Art. no. e57848. [Online]. Available: https://periodicos.uem.br/ojs/index.php/ActaSciTechnol/article/view/

[2] A. Haddadi, E. Farantatos, I. Kocar, and U. Karaagac, "Impact of inverter based resources on system protection," *Energies*, vol. 14, no. 4, p. 1050, Feb. 2021. [Online]. Available: https://www.mdpi.com/1996-1073/14/4/1050

[3] M. Bini, R. Abboud, P. Lima, and F. Lollo, "Challenges and solutions in the protection of transmission lines connecting nonconventional power sources," Schweitzer Engineering Laboratories, Pullman, WA, USA, Tech. Rep. TP7011-01, 2021.

[4] R. Chowdhury and N. Fischer, "Transmission line protection for systems with inverter-based resources—Part I: Problems," *IEEE Trans. Power Del.*, vol. 36, no. 4, pp. 2416–2425, Aug. 2021.

[5] M. J. B. B. Davi, M. Oleskovicz, and F. V. Lopes, "A review of signal processing for fault diagnosis in systems with inverter-based resources and an improved high-frequency component-based disturbance detector," *Electric Power Syst. Res.*, vol. 236, Nov. 2024, Art. no. 110938, doi: 10.1016/j.epsr.2024.110938.

[6] K. Al Kharusi, A. El Haffar, and M. Mesbah, "Fault detection and classification in transmission lines connected to inverter-based generators using machine learning," *Energies*, vol. 15, no. 15, p. 5475, Jul. 2022.

[7] M. J. B. B. Davi, M. Oleskovicz, and F. V. Lopes, "An impedance-multi-method-based fault location methodology for transmission lines connected to inverter-based resources," *Int. J. Electr. Power Energy Syst.*, vol. 154, Dec. 2023, Art. no. 109466.

[8] S. R. Mohanty, A. K. Pradhan, and A. Routray, "A cumulative sum-based fault detector for power system relaying application," *IEEE Trans. Power Del.*, vol. 23, no. 1, pp. 79–86, Jan. 2008.

[9] K. Nagaraju, P. S. V. S. T. Varma, and B. R. K. Varma, "A current-slope based fault detector for digital relays," in *Proc. Annu. IEEE India Conf.*, India, Dec. 2011, pp. 1–4.

[10] M. Saha and E. Rosolowski, *Fault Location on Power Networks*. Cham, Switzerland: Springer, 2010.

[11] B. Rathore and M. Singh, "Stockwell transform based decision tree for transmission line fault diagnosis," in *Proc. IEEE 13th Int. Conf. Ind. Inf. Syst. (ICIIS)*, Dec. 2018, pp. 427–431.

[12] V. P. Goli and S. Das, "A transient current based DG interconnected transmission system protection scheme using wavelet analysis," in *Proc. IEEE Kansas Power Energy Conf. (KPEC)*, Jul. 2020, pp. 1–6.

[13] A. Kulshrestha, O. P. Mahela, and M. Kumar Gupta, "A discrete wavelet transform and rule based decision tree based technique for identification of fault in utility grid network with wind energy," in *Proc. Int. Conf. Adv. Electr., Comput., Commun. Sustain. Technol. (ICAECT)*, Feb. 2021, pp. 1–6.

[14] G. Kapoor, A. Yadav, and G. Jain, "Protection of wind park incorporated series compensated transmission line using DMWT," in *Proc. 1st Int. Conf. Power, Control Comput. Technol. (ICPC2T)*, Jan. 2020, pp. 149–154.

[15] F. V. Lopes, W. L. A. Neves, and D. Fernandes, "A TDQ-based fault detector for digital power system relaying," in *Proc. IEEE PES Gen. Meeting | Conf. Expo.*, Jul. 2014, pp. 1–5.

[16] E. Muljadi, S. Pasupulati, A. Ellis, and D. Kosterov, "Method of equivalencing for a large wind power plant with multiple turbine representation," in *Proc. IEEE Power Energy Soc. Gen. Meeting - Convers. Del. Electr. Energy 21st Century*, Jul. 2008, pp. 1–9.

[17] R. H. Tan and V. K. Ramachandaramurthy, "Numerical model framework of power quality events," *Eur. J. Sci. Res.*, vol. 43, no. 1, pp. 30–47, 2010.

[18] J. J. Tomic, M. D. Kusljevic, and V. V. Vujicic, "A new power system digital harmonic analyzer," *IEEE Trans. Power Del.*, vol. 22, no. 2, pp. 772–780, Apr. 2007.

[19] A. Guzmán, M. V. Mynam, V. Skendzic, J. L. Eternod, and R. M. Morales, "Directional elements—How fast can they be?" in *Proc. XIV Simposio Iberoamericano Sobre Proteccion de Sistemas Electricos de Potencia*, Feb. 2019, pp. 1–16.

[20] S. Gautam and S. M. Brahma, "Overview of mathematical morphology in power systems—A tutorial approach," in *Proc. IEEE Power Energy Soc. Gen. Meeting*, Jul. 2009, pp. 1–7.

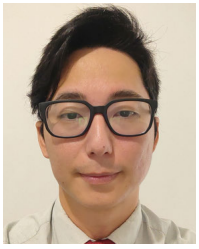

SÓLON S. OTOMURA received the B.Sc. degree in electrical engineering from the Federal University of Mato Grosso (UFMT), Brazil, in 2015. He is currently pursuing the M.Sc. degree in electrical engineering with São Carlos School of Engineering (EESC), University of São Paulo (USP), Brazil. His research focuses on fault detection and classification in wind farms. His areas of expertise include power system protection, modeling, and simulation of wind power systems. His research interests include fault diagnosis, power system transients, distributed generation systems, and wind energy systems.

MOISÉS J. B. B. DAVI received the B.Sc. degree in electrical engineering and the M.Sc. degree in technological innovation from the Federal University of Triângulo Mineiro, in 2014 and 2021, respectively, and the Ph.D. degree in electrical engineering from São Carlos School of Engineering (EESC), University of São Paulo (USP), Brazil, in 2025. He has extensive experience in power system protection, IED commissioning, transient electromagnetic simulation and analysis, and oscillography interpretation. His research interests include protective relaying, power system transients, advanced power system modeling, fault location techniques, and the control and protection of renewable energy systems.

MATHEUS DO VAL OLIVEIRA received the B.Sc. degree in electrical engineering, with emphasis on power systems and automation from São Carlos School of Engineering (EESC), University of São Paulo (USP), Brazil, in 2023, where he is currently pursuing the M.Sc. degree in electrical engineering. His research interests include the protection of transmission and distribution lines using deep learning techniques.

JOSÉ C. M. VIEIRA (Member, IEEE) received the M.Sc. and Ph.D. degrees in electrical engineering from the University of Campinas, Campinas, Brazil, in 1999 and 2006, respectively. From 1999 to 2003, he was a Consulting Engineer with Figener, Sao Paulo, Brazil. He is currently an Associate Professor with São Carlos School of Engineering, São Carlos, Brazil. His research interests include power distribution systems, integration of distributed energy resources, and power system protection.

MÁRIO OLESKOVICZ (Member, IEEE) received the degree in electrical engineering from the Federal University of Santa Catarina (UFSC), Brazil, in 1995, and the M.Sc. and Ph.D. degrees in electrical engineering from Sao Carlos Engineering School (EESC), University of Sao Paulo (USP), Brazil, in 1997 and 2001, respectively. He is currently an Assistant Professor with the Department of Electrical and Computer Engineering, EESC, USP. He works in the electrical engineering area, focusing on power systems (generation, transmission, distribution, and microgrids), power quality, and digital protection of power systems.

Coordenação de Aperfeiçoamento de Pessoal de Nível Superior (CAPES) - ROR identifier: 00x0ma614